

Role of model ingredients in the production of light particles and entropy

Sukhjit Kaur and Rajeev K. Puri*

Department of Physics, Panjab University, Chandigarh 160 014, India

(Received 21 March 2014; published 30 September 2014)

We study the role of different entrance channels and model ingredients on the composite particle yield ratios and entropy production. We find that the composite particle yield ratios show some sensitivity towards equation of state. The Gaussian width of the nucleons affects the production of light charged particles significantly.

DOI: [10.1103/PhysRevC.90.037602](https://doi.org/10.1103/PhysRevC.90.037602)

PACS number(s): 25.70.Pq, 24.10.Cn

Various phenomena occurring from low to high incident energies such as fusion, cluster decay, multifragmentation, and collective and elliptic flows are found to be sensitive towards incident energy, system size, isospin asymmetry, and impact parameter of the reaction [1–8]. At intermediate energies, model ingredients (such as equation of state, nucleon nucleon (nn) cross section, Gaussian width, etc.) also affect the dynamics apart from the above factors [7–12]. For example, studies reported in Refs. [2,6,8–11] deal with the effects of different entrance channels and model ingredients on the fragmentation pattern. Nagamiya *et al.* [13] measured the cross section for the production of light fragments and pions and found that the yield ratios of the composite fragments to protons depend on the projectile and target masses and incident beam energy. One of us and coworkers studied the role of different nn cross sections on the production of fragments [12] and concluded that nn cross section has significant effect in peripheral collisions whereas nearly no effect was found for central collisions. Similarly, the width of the Gaussian also plays a significant role in the fragment formation. It can affect fragmentation by ~ 30 – 50% [9,10]. Recently, it has been found that the wavepacket width also affects the stability and central densities of the initial nuclei as well as formation and stability of the fragments [11].

Light cluster production has captured a lot of attention recently [14–16]. Doss *et al.* [17] measured the yield ratios of the light clusters ($A < 5$) to protons at incident energies between 150 and 1050 MeV/nucleon and fitted data with the quantum statistical model (QSM). A good agreement was reported for the calculations except at 150 MeV/nucleon. These composite clusters such as d , t , ^3He , and ^4He have also been used to extract entropy produced during a collision. Interestingly, entropy was found to stay constant during the expansion phase and therefore is an excellent candidate for getting information about the early phase of the reaction. Earlier, Aichelin *et al.* [18] studied the role of momentum-dependent interactions (MDI) and equations of state (EOS) on the deuteron-to-proton (d/p) ratio. They found that though d/p ratio is insensitive to MDI, it has weaker sensitivity towards EOS for heavier systems. Puri and coworkers [19,20] studied the entropy and light cluster production at intermediate energies and found that the composite particle yield ratios and entropy are insensitive to the momentum-dependent

interactions as well as to various factors governing the isospin effects. The ratio of the deuteronlike to protonlike clusters and entropy is, however, affected by the isospin asymmetry. As evident from the above, a complete systematic study of the dependence of entropy production on various entrance channels and model ingredients is still missing. Since light particle production is an important channel for the reaction dynamics, it is worth analyzing it systematically. Our present aims, therefore, are (i) to compare our theoretical calculations with experimental data for the yield ratios of various clusters over wide range of incident energies, masses, and impact parameter and (ii) to present a complete systematic analysis of the light particles as well as entropy production with respect to various model ingredients.

The present study is made within the framework of isospin-dependent quantum molecular dynamics (IQMD) model [21]. The phase space generated with the IQMD model is stored at different time steps and clusterized using the minimum spanning tree (MST) method [22]. Here, the ratio of the composite particles to protons, X/p , is calculated in following way:

$$X/p = Y(A = 2, 3, \text{ and } 4)/p, \quad (1)$$

where $Y(A = m)$ stands for the number of fragments with mass m in one event and p represents the number of protons and is calculated as

$$p = \frac{Z_P + Z_T}{A_P + A_T} [Y(A = 1)], \quad (2)$$

where $Z_P + Z_T$ and $A_P + A_T$, respectively, define the total charge and mass of the colliding system. In many studies, one uses participant proton multiplicity, N_p and deuteronlike and protonlike clusters rather than using protons and composite particles. The deuteronlike and protonlike ratio can further be used for estimating the entropy production. For the details, we refer the reader to Refs. [19,20,23–25].

For the present study, the reactions of $^{20}\text{Ne}+^{20}\text{Ne}$, $^{40}\text{Ca}+^{40}\text{Ca}$, $^{93}\text{Nb}+^{93}\text{Nb}$, $^{145}\text{Nd}+^{145}\text{Nd}$, $^{197}\text{Au}+^{197}\text{Au}$, and $^{238}\text{U}+^{238}\text{U}$ are simulated at energies between 150 and 1050 MeV/nucleon and over the entire range of the impact parameter. The role of the equation of state (EOS) was analyzed by using soft, hard, and soft momentum-dependent (SMD) equations of state along with full and reduced (20%) energy- and isospin-dependent nn cross sections. Here, apart from the standard mass-dependent Gaussian width, we have also taken two fixed Gaussian widths, i.e., $4L = 4.33 \text{ fm}^2$ (narrow) and

*rkpuri@pu.ac.in

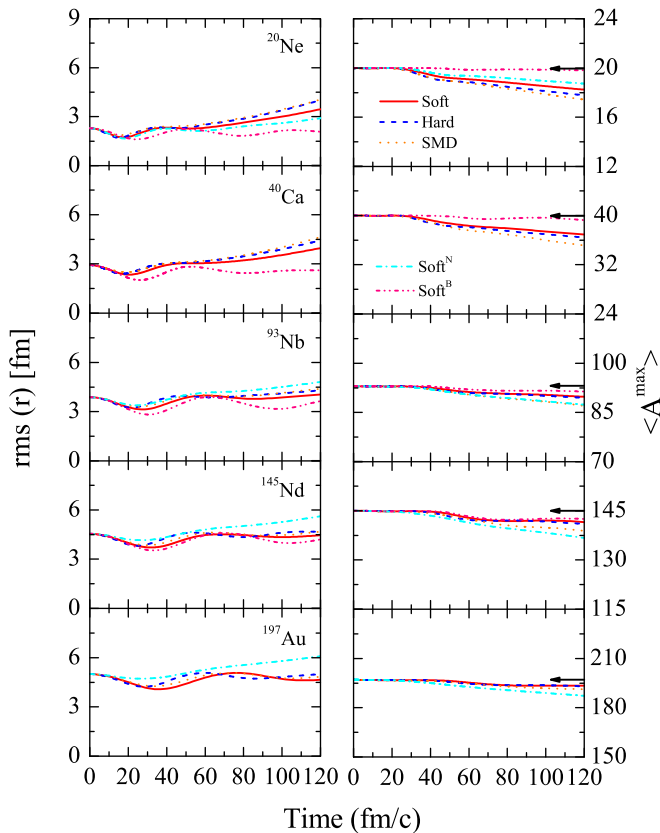


FIG. 1. (Color online) The time evolution of rms (r) radius and heaviest fragment, $\langle A^{\text{max}} \rangle$ for various nuclei ^{20}Ne , ^{40}Ca , ^{93}Nb , ^{145}Nd , and ^{197}Au . Solid, dashed, dotted, dash-dotted, and dash-double-dotted lines represent the results for soft, hard, SMD, soft with narrow Gaussian, and soft with broader Gaussian, respectively.

$4L = 8.66 \text{ fm}^2$ (broader). It is worth mentioning that the width of the Gaussian has always been a subject of heavy debate in the literature. Many authors take fixed Gaussian widths whereas others advocate system-dependent or time-dependent widths. It is worth mentioning that all simulations are carried out by reducing the Fermi momentum by 30%. All composite particle yield ratios are computed after the compression phase is over and nucleonic density gets saturated (i.e., at 40 fm/c). The participant proton multiplicity, N_p , is calculated at a slightly later time (i.e., at 100 fm/c). Before presenting results, it is important to look for the stability aspect of various nuclei. In Fig. 1, we display the time evolution of root mean square (rms) radius as well as of heaviest size of the nuclei identified by the MST method. It is evident from the figure that nuclei generated and propagating under the influence of various equations of state, i.e., soft, hard, soft momentum-dependent as well as with narrow and broader Gaussians, have stable rms radii and the heaviest mass is close to the mass of the nucleus in question. One finds that in all cases rms radius and heaviest size are close to mean values. The broader Gaussian generates heavier size close to the size of the nucleus, though is less bound compared to the one generated by narrow width. Before analyzing the role of model ingredients, let us compare our results with experimental data.

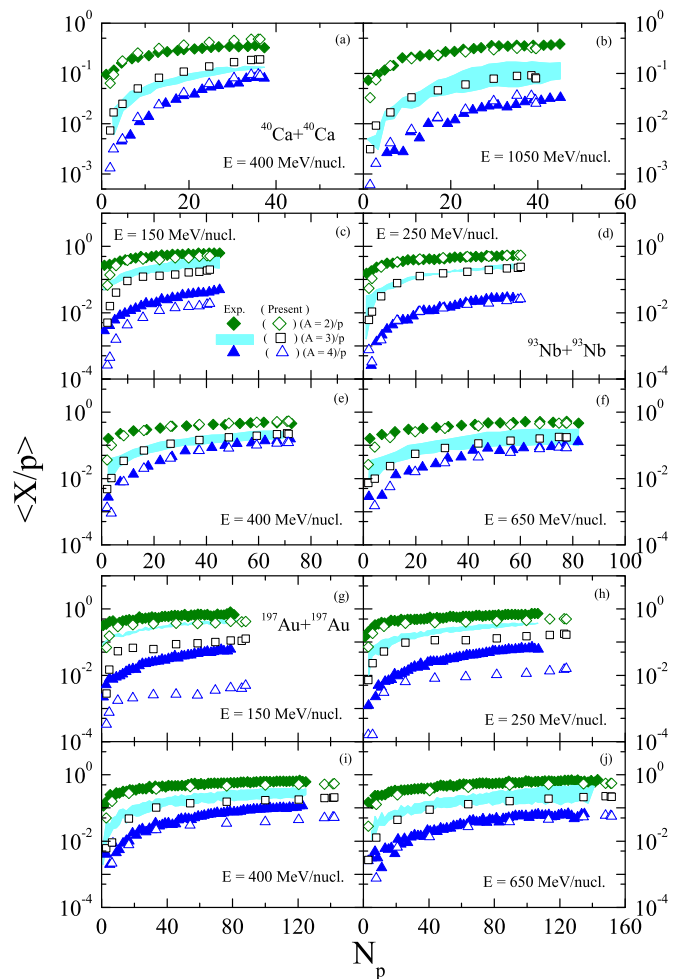


FIG. 2. (Color online) The composite particle yield ratios, X/p , where X stands for $A = 2$ (\diamond), $A = 3$ (\square), and $A = 4$ (\triangle) in panels (a), (b), (e), and (f); $A = 2$ (\diamond), $A = 3$ (\square), and $0.2 A = 4$ (\triangle) in panels (c), (d), and (h); $A = 2$ (\diamond), $A = 3$ (\square), and $0.1 A = 4$ (\triangle) in panel (g); and $A = 2$ (\diamond), $A = 3$ (\square), and $0.5 A = 4$ (\triangle) in panels (i) and (j) as a function of participant proton multiplicity, N_p , for reactions of $^{40}\text{Ca}+^{40}\text{Ca}$, $^{93}\text{Nb}+^{93}\text{Nb}$, and $^{197}\text{Au}+^{197}\text{Au}$. Solid diamonds and triangles represent the experimental normalized d/p and $^4\text{He}/p$ ratios, respectively [17]. The shaded region enclosed the experimental yield ratios of t/p and $^3\text{He}/p$ [17].

In Fig. 2, we display the composite particle yield ratios (X/p ; X stands for $A = 2, 3$ and 4) as a function of participant proton multiplicity, N_p for the reactions of $^{40}\text{Ca}+^{40}\text{Ca}$, $^{93}\text{Nb}+^{93}\text{Nb}$, and $^{197}\text{Au}+^{197}\text{Au}$ using standard Gaussian widths. The open (solid) symbols represent our calculations (experimental data [17]). From the figure, we see that X/p ratio increases with participant proton multiplicity, N_p (or decreases with the impact parameter). The X/p ratio increases sharply with N_p for semicentral and peripheral collisions and reaches asymptotic value for higher values of N_p , i.e., for central collisions. From the figure, we see that our calculations are in good agreement with experimental data [17] covering masses from 80 to 400 units and incident energies from 150 to 1050 MeV/nucleon. Some disagreement can be seen in the low energy reactions of $^{197}\text{Au}+^{197}\text{Au}$. The overall

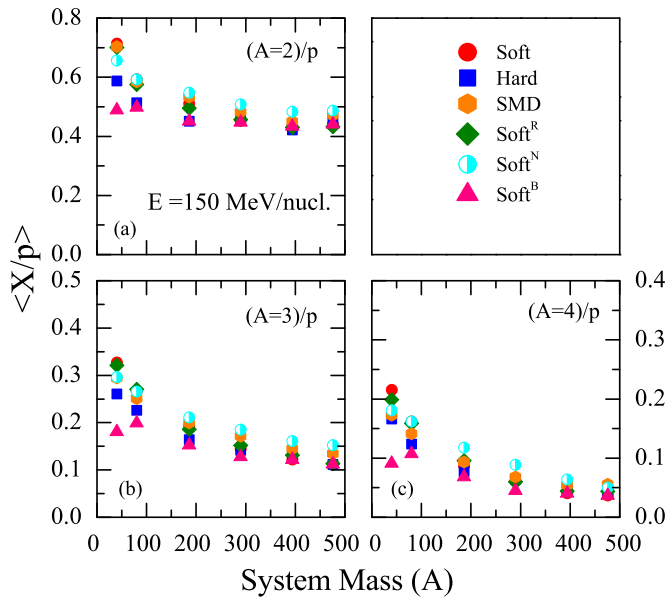


FIG. 3. (Color online) The composite particle yield ratios as a function of composite system mass at incident energy of 150 MeV/nucleon. Various symbols are explained in the text. Here, reactions are for central geometries only.

agreement guarantees that the IQMD model contains essential ingredients and can be used to analyze the role of model ingredients. It is worth mentioning that the IQMD model [21] has several different ingredients compared to the QMD model [22] that can lead to different results.

In Fig. 3, we display the system size dependence of the composite particle yield ratios at incident energy of 150 MeV/nucleon for central collisions only ($b/b_{\max} = 0.0-0.2$). The solid circles, squares, diamonds, hexagons, half-filled circles, and solid triangles represent calculations using soft, hard, soft along with reduced cross section (Soft^R), SMD, soft with narrow (Soft^N), and soft with broader (Soft^B) Gaussian widths, respectively. From the figure, we see that the composite particle yield ratios are very sensitive to the width of the Gaussian irrespective of the mass of the system. In lighter systems, some sensitivity towards equation of state can also be seen. Nearly no effect is visible for the medium and heavy masses towards different equations of state as well as its momentum dependence and reduced cross section. The effect of different Gaussian widths, however, remains visible even for medium and heavy masses. We see that for lighter systems, composite particle yield ratios are larger in the case of the soft equation of state compared to that of the hard equation of state. This can be attributed to the fact that soft matter is easily compressible, which results in greater density and hence leads to higher value of the composite yield ratios. Further, as noted, broader width of the Gaussian causes decrease in the composite particle yield ratios. An extended wave packet has larger interaction range and it will connect large number of nucleons in a fragment that will generate more heavier fragments. Hence, the yield of the light fragments will eventually decrease with the width of the Gaussian. On the other hand, nn cross section and MDI

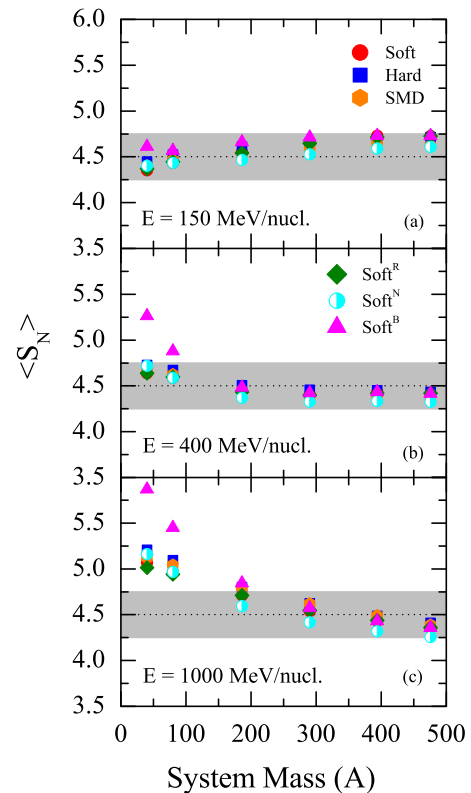


FIG. 4. (Color online) The entropy ($\langle S_N \rangle$) per nucleon as a function of composite system mass for the central collisions at incident energies 150 (upper), 400 (middle), and 1000 (lower panels) MeV/nucleon. Symbols have the same meaning as in Fig. 3.

have negligible roles to play. In central collisions, excitation energy is too high to have a role of different cross sections and momentum-dependent interactions. It is worth mentioning that ALADIN Collaboration [26] has also measured and analyzed yields and double ratios of various light clusters in the reaction of Au with various targets ranging from C to Pb.

Since the light cluster production is also related to the entropy production, it would be interesting to see the effect of various model ingredients on the entropy production. In Fig. 4, we display the system size dependence of the entropy production for various model ingredients at incident energies of 150 (upper panel), 400 (middle panel), and 1000 (lower panel) MeV/nucleon for central collisions only. Symbols have the same meaning as in Fig. 3. From the figure, we see that the entropy is insensitive to the EOS, momentum-dependent interactions, and nn cross section, but it shows sensitivity towards the width of the Gaussian. The effect is more prominent at higher incident energies for lighter systems. As noted, entropy ($\langle S_N \rangle$) is nearly independent of the system size at 150 MeV/nucleon, whereas one sees significant dependence at 1000 MeV/nucleon. Since the fragments produced in the reaction of $^{20}\text{Ne}+^{20}\text{Ne}$ are close to d_{like} clusters, further increase in the incident energy breaks them into free nucleons. This not only decreases the number of d_{like} clusters but will also increase p_{like} clusters that leads to net fall in the ratio of the $d_{\text{like}}/p_{\text{like}}$ clusters and hence rise in the entropy production.

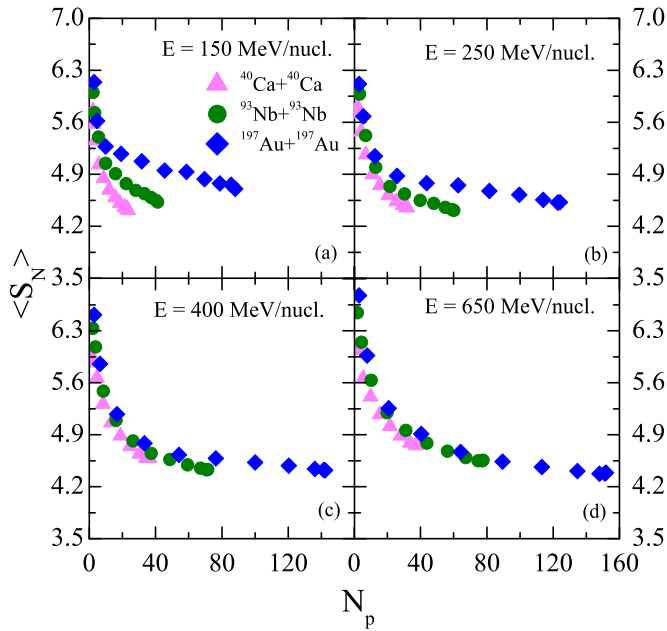


FIG. 5. (Color online) The entropy $\langle S_N \rangle$ per nucleon as a function of participant proton multiplicity, N_p . Various symbols are explained in the text.

On the other hand, in the case of heavier nuclei, intermediate fragments break into free nucleons and d_{like} clusters, therefore keeping their ratio nearly unaffected.

In Fig. 5, we display entropy as a function of participant proton multiplicity, N_p for reactions of $^{40}\text{Ca}+^{40}\text{Ca}$, $^{93}\text{Nb}+^{93}\text{Nb}$, and $^{197}\text{Au}+^{197}\text{Au}$ at incident energies of 150, 250, 400, and 650 MeV/nucleon. The solid triangles, circles, and diamonds represent the calculations for the reactions of $^{40}\text{Ca}+^{40}\text{Ca}$, $^{93}\text{Nb}+^{93}\text{Nb}$, and $^{197}\text{Au}+^{197}\text{Au}$, respectively. We find that entropy decreases with participant proton multiplicity (increases with impact parameter), indicating more entropy production in peripheral collisions compared to central collisions. We see that the entropy is slightly more in the case of a heavy system compared to a lighter one at lower incident energies. This difference reduces as incident energy increases.

Summarizing, we studied the effect of different entrance channels and model ingredients on the composite particle yield ratios and entropy production. We found that the composite particle yield as well as entropy for the central collisions are insensitive to nn cross section and momentum-dependent interactions. The composite particle yield ratios show some sensitivity towards equation of state. The Gaussian width, however, seems to have a significant effect on the production of light charged particles.

This work is supported by a research grant from the Council of Scientific and Industrial Research (CSIR), GOI Vide Sanction No. 03(1263)/12/EMR-II. S.K. acknowledges fellowship from the Department of Science and Technology, GOI.

- [1] R. K. Puri and R. K. Gupta, *J. Phys. G: Nucl. Part. Phys.* **18**, 903 (1992); I. Dutt and R. K. Puri, *Phys. Rev. C* **81**, 064609 (2010); **81**, 064608 (2010).
- [2] J. K. Dhawan and R. K. Puri, *Phys. Rev. C* **75**, 057901 (2007).
- [3] J. Łukasik *et al.*, *Phys. Lett. B* **608**, 223 (2005).
- [4] R. Popescu *et al.*, *Phys. Lett. B* **331**, 285 (1994).
- [5] Q. Pan and P. Danielewicz, *Phys. Rev. Lett.* **70**, 2062 (1993).
- [6] C. A. Ogilvie *et al.*, *Phys. Rev. Lett.* **67**, 1214 (1991); M. B. Tsang *et al.*, *ibid.* **71**, 1502 (1993).
- [7] S. Gautam *et al.*, *J. Phys. G: Nucl. Part. Phys.* **37**, 085102 (2010).
- [8] J. Singh, S. Kumar, and R. K. Puri, *Phys. Rev. C* **62**, 044617 (2000).
- [9] S. Kaur and A. D. Sood, *Phys. Rev. C* **82**, 054611 (2010).
- [10] Rajni and S. Kumar, *Eur. Phys. J. A* **48**, 19 (2012).
- [11] C. Li, J. Tian, L. Ou, and N. Wang, *Phys. Rev. C* **87**, 064615 (2013).
- [12] S. Kumar, R. K. Puri, and J. Aichelin, *Phys. Rev. C* **58**, 1618 (1998).
- [13] S. Nagamiya *et al.*, *Phys. Rev. C* **24**, 971 (1981).
- [14] J. K. Dhawan, N. Dhiman, A. D. Sood, and R. K. Puri, *Phys. Rev. C* **74**, 057901 (2006).
- [15] L. W. Chen, C. M. Ko, and B. A. Li, *Phys. Rev. C* **68**, 017601 (2003).
- [16] F. Gagnon-Moisan *et al.*, *Phys. Rev. C* **86**, 044617 (2012).
- [17] K. G. R. Doss *et al.*, *Phys. Rev. C* **32**, 116 (1985); **37**, 163 (1988).
- [18] J. Aichelin, A. Rosenhauer, G. Peilert, H. Stoecker, and W. Greiner, *Phys. Rev. Lett.* **58**, 1926 (1987).
- [19] Y. K. Vermani and R. K. Puri, *Nucl. Phys. A* **847**, 243 (2010).
- [20] S. Kaur and R. K. Puri, *Phys. Rev. C* **89**, 057603 (2014).
- [21] C. Hartnack *et al.*, *Eur. Phys. J. A* **1**, 151 (1998); R. Bansal, S. Gautam, and R. K. Puri, *J. Phys. G: Nucl. Part. Phys.* **41**, 035103 (2014).
- [22] J. Aichelin, *Phys. Rep.* **202**, 233 (1991).
- [23] P. J. Siemens and J. I. Kapusta, *Phys. Rev. Lett.* **43**, 1486 (1979).
- [24] G. Bertsch and J. Cugnon, *Phys. Rev. C* **24**, 2514 (1981); G. Bertsch, *Nucl. Phys. A* **400**, 221C (1983).
- [25] G. Peilert *et al.*, *Phys. Rev. C* **39**, 1402 (1989).
- [26] M. Begemann-Blaich *et al.*, *Phys. Rev. C* **58**, 1639 (1998); W. Trautmann, R. Bassini, M. Begemann-Blaich, A. Ferrero, S. Fritz, S. J. Gaff-Ejakov, C. Gross, G. Imme, I. Iori, and U. Kleinevoss *et al.*, *ibid.* **76**, 064606 (2007).